

mmCooper: A Multi-agent Multi-stage Communication-efficient and Collaboration-robust Cooperative Perception Framework

Bingyi Liu¹, Jian Teng¹, Hongfei Xue^{2*}, Enshu Wang^{3*}, Chuanhui Zhu¹, Pu Wang², Libing Wu³
¹Wuhan University Of Technology, ²University of North Carolina at Charlotte, ³Wuhan University

{byliu, tengjian, zhuchuanhui}@whut.edu.cn,

{hongfei.xue, Pu.Wang}@charlotte.edu, {wanges17, wu}@whu.edu.cn

Abstract

Collaborative perception significantly enhances individual vehicle perception performance through the exchange of sensory information among agents. However, real-world deployment faces challenges due to bandwidth constraints and inevitable calibration errors during information exchange. To address these issues, we propose mm-Cooper, a novel multi-agent, multi-stage, communication-efficient, and collaboration-robust cooperative perception framework. Our framework leverages a multi-stage collaboration strategy that dynamically and adaptively balances intermediate- and late-stage information to share among agents, enhancing perceptual performance while maintaining communication efficiency. To support robust collaboration despite potential misalignments and calibration errors, our framework prevents misleading low-confidence sensing information from transmission and refines the received detection results from collaborators to improve accuracy. The extensive evaluation results on both real-world and simulated datasets demonstrate the effectiveness of the mm-Cooper framework and its components.

1. Introduction

With the advancement of autonomous driving systems[19, 57], perception devices such as cameras and LiDARs have been widely deployed. Although perception technologies have witnessed rapid advancements driven by deep learning-based algorithms, the traditional single-vehicle perception paradigms [23, 30, 52] cannot meet the safety and reliability requirements of autonomous vehicles due to unavoidable factors such as object occlusion and limitations in detection range [1, 6, 14, 27, 61].

Benefiting from infrastructure improvements and the advancement of Internet of Vehicles (IoVs) technologies like V2X [25, 26], autonomous vehicles can achieve multi-vehicle collaborative perception by sharing perception in-

formation [5, 47], which significantly enhances the performance of perception systems. Although cooperative perception has made progress recently, its practical deployment still faces challenges such as communication resource constraints [8, 13], localization errors [31, 34], and low information fusion efficiency [46, 55].

In cooperative perception systems, the effectiveness of fusion strategies significantly affects both perception performance and communication efficiency. The fusion strategies can be divided into three categories: early, intermediate, and late fusion methods. Specifically, early fusion methods [7, 61] aggregate raw sensor observations from all agents, providing abundant information but requiring immense bandwidth, making this approach costly for communication. Intermediate fusion methods [8, 13, 53–55] partially mitigate this issue by sharing encoded features rather than raw data to reduce communication overhead. However, transmitting the feature map of the entire sensing scenario still results in substantial bandwidth consumption [13]. Late fusion methods [38, 40] on the other hand, minimize communication demands by sharing lightweight perception results among agents. However, this approach is highly sensitive to environmental noise, as even minor disturbances can degrade collaborative quality [31]. Overall, these above single-stage cooperative perception approaches face challenges in managing the trade-off between perception accuracy and communication efficiency, raising a compelling question: *Can we improve the perception performance while preserving communication efficiency by strategically sharing information across multiple stages to harness the strengths of each fusion stage?*

In addition, the data exchanged by agents inevitably experiences misalignment and contains calibration errors during the synchronization process due to communication delays and pose noise [15, 41]. These calibration errors can produce misleading features and proposals in subsequent steps, thereby affecting the performance of the perception system. While existing intermediate fusion methods attempt to address the calibration errors through position-

*Corresponding authors

wise feature fusion [20, 22, 29], they often overlook the critical role of neighboring region information for enhancing collaborative robustness. Meanwhile, late fusion methods [3, 36, 42] simply merge bounding boxes from collaborative agents, failing to leverage information-rich intermediate features from the ego agent, which could help refine and calibrate these bounding boxes for higher accuracy.

To this end, we propose **mmCooper**, a novel multi-agent, multi-stage, communication-efficient, and collaboration-robust **cooperative** perception framework. The proposed mmCooper framework facilitates effective information aggregation across fusion stages and enhances communication efficiency through carefully designed core components. Specifically, we design an adaptive multi-stage data fusion mechanism that facilitates multi-agent cooperation by dynamically fusing information at both intermediate and late stages. Guided by a confidence-based filtering strategy, this mechanism automatically assesses and determines the data volume to be processed at intermediate and late stages. High-confidence bounding boxes are shared directly, while intermediate features are selectively shared instead of bounding boxes for regions requiring further contextual reference, and low-confidence areas are excluded to prevent propagating misleading information. This dual-stage fusion approach enhances perception performance while maintaining communication efficiency.

Besides, to further address potential misalignment and calibration noise among agents, we incorporate specific designs in the proposed mmCooper framework for both intermediate and late stages. In the intermediate stage, we introduce a Multi-scale Offset-aware Fusion Module that not only fuses data from target locations related to cooperative agents' views but also from nearby regions, adding redundancy to mitigate calibration noise. For the late stage, we design a Bounding Box Filtering & Calibration Module that uses the information-rich intermediate-stage features from the ego agent to filter inaccurate bounding boxes received from other agents and refine the remaining noisy ones. By integrating these corrected and ego-generated bounding boxes, our mmCooper framework can achieve high perception accuracy and robustness. To summarize, our main contributions are summarized as follows:

- We propose mmCooper, a multi-agent multi-stage communication-efficient collaboration-robust cooperative perception framework. To our knowledge, this is the first framework to address the tradeoff between limited communication bandwidth and desired perception performance by sharing both intermediate and late-stage information for multi-agent collaborative perception.
- To address the potential misalignment and calibration error among agents, we design a Multi-scale Offset-aware Fusion Module to integrate spatially adjacent contextual information at different feature scales in the intermediate

stage and a Bounding Box Filtering & Calibration Module to filter and improve the bounding boxes from other agents in the late stage, guided by the information-rich intermediate features.

- Extensive experiments show excellent performance on both real-world and simulated datasets, with a 7.29%/1.31%/2.09% improvement in AP@0.7 on OPV2V[50], DAIR-V2X[56] and V2XSet[49] datasets over the second-best SOTA methods. Meanwhile, our approach requires only 1/9153, 1/156, and 1/18305 of the communication volume used by comparable methods. Furthermore, our method consistently outperforms previous approaches under various configurations.

2. Related Work

2.1. Multi-Agent Communication

Communication strategies in multi-agent systems have been widely studied [39]. Early works [21, 37, 44] often used predefined protocols or heuristic methods to determine how agents communicate with each other. However, these methods are difficult to generalize to complex tasks. Recently, several learning-based communication strategies have been proposed to adapt to diverse scenario applications. For instance, Vain [12] utilizes attention neural structures to specify the information that needs to be shared in agent interactions. ATOC [17] introduces recurrent units to decide who agents communicate with by receiving local observations and action intentions from other agents. TarMAC [9] designs an architecture oriented towards reinforcement learning, learning to communicate from task-specific rewards. CommNet [43] learns continuous communication in multi-agent systems. Most of these previous works have considered decision-making tasks and have employed reinforcement learning due to the lack of explicit supervision. Different from these works, our paper focuses on LiDAR-based 3D perception tasks in complex autonomous driving scenarios and achieves efficient communication between agents using a multi-stage communication strategy.

2.2. Collaborative Perception

Collaborative perception addresses the limitations of single-agent perception by aggregating perception information from surrounding agents to adapt to complex and dynamic autonomous driving environments. Current work is categorized into early, intermediate, and late fusion based on collaboration stages. Early fusion [7, 59, 61] shares raw point cloud data among agents, achieving high perception performance but consuming significant bandwidth resources. EMP [61] achieved scalability and adaptability on highly fluctuating open roads by dynamically partitioning the point cloud range shared by agents. Late fusion [38, 40, 51] shares lightweight proposals between agents but performs poorly and is sensitive to noise. VIPS [38] implemented efficient graph-structured matching to enable object-level

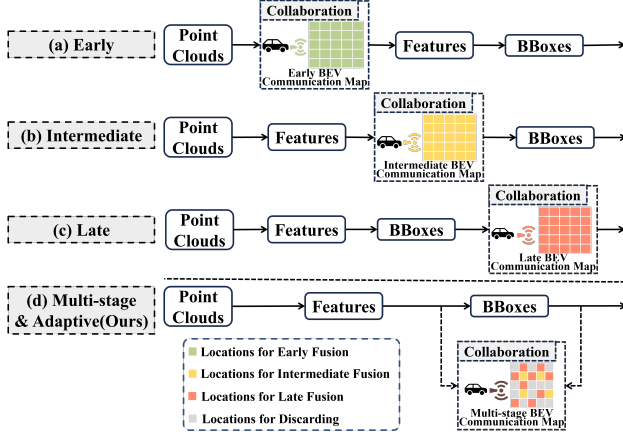


Figure 1. Comparison between our proposed multi-stage mmCooper framework and existing methods. The BEV (Bird’s Eye View) communication map illustrates the information shared by agents at each scene location. (a)(b)(c) depict existing methods, which transmit the entire scene’s data in a single stage without considering sensing confidence, leading to excessive communication overhead and degraded performance. (d) demonstrates how mmCooper selectively transmits non-overlapping information across multiple stages, reducing communication costs and enhancing model performance.

fusion. Intermediate fusion [13, 22, 29, 49, 58] shared features among agents, yet complete Intermediate features still incur high bandwidth consumption. Recent work focused on novel communication mechanisms to filter Intermediate features and reduce communication volume. For instance, Where2comm [13] employed a confidence-based scheme to guide agents in focusing on sharing spatially critical information. ERMVP [58] adopted a hierarchical feature sampling strategy to reduce communication overhead while leveraging sparse consensus features to mitigate localization errors. Different from these works, our framework conducts multi-stage fusion instead of single-stage fusion which balances the perception performance and communication overhead. As far as we know, only a few works have considered multi-stage settings. Zhang *et al.* [60] proposes a defense method that combines raw data and intermediate features to fuse redundant information, thereby reducing the impact of spurious data. However, this work focuses on security issues related to collaborative perception instead of improving sensing performance. Xie *et al.* [48] applies reinforcement learning for dynamic partitioning of early, intermediate, and late-stage information. However, this work merely divides the data without integrating information across stages. In contrast to these works, this paper introduces a collaborative perception framework that aims to improve sensing performance by conducting multi-stage data fusion.

3. Methodology

3.1. Overview

As illustrated in Fig. 1, our key idea is to conduct selective multi-stage agent collaboration, rather than the single-

stage fusion used in existing methods. Conventional approaches indiscriminately transmit data encompassing the entire scene through a single stage, introducing undesired low-quality sensing information during communication. This not only increases communication overhead but also complicates fusion, as the system must first evaluate the quality of received data to ensure reliable results. In contrast, our approach adopts a selective multi-stage collaboration strategy, where the transmission decision, whether to send data and at which stage, is determined based on the sensing confidence level of each location. For high-confidence regions, we transmit late-stage bounding boxes, minimizing communication costs. For moderate-confidence regions, we transmit intermediate-stage features for richer information. For low-confidence regions, transmission is suppressed to prevent misleading other agents. Additionally, our framework incorporates alignment and calibration corrections during both intermediate and late-stage fusion, further enhancing the reliability of the fused results.

The details of our proposed mmCooper framework are illustrated in Fig. 2, which comprises three main components: (1) the Information Broadcasting, (2) the Intermediate-stage Fusion, and (3) the Late-stage Fusion. The encoded point cloud features will be sent to two branches. In one branch, the Information Broadcasting (Sec. 3.3) employs a Confidence-based Filter Generation Module to dynamically determine whether data should be suppressed, transmitted at the intermediate stage, or transmitted at the late stage. In the other branch, the Intermediate-stage Fusion (Sec. 3.4) contains the Multi-scale Offset-aware Fusion Module, which uses cross-attention to integrate features from both target and neighboring regions. This module mitigates potential misalignment between features from the ego and other agents, ensuring robust feature fusion. In Late-stage Fusion (Sec. 3.5), a BBox Filtering & Calibration Module removes inaccurate bounding boxes from other agents and refines the remaining ones using the ego agent’s information-rich intermediate features. The calibrated bounding boxes from all agents will be merged with those generated by the ego agent to produce the final outputs.

3.2. Observation Encoding

In a multi-agent cooperative perception scenario, consider the collaboration of n agents, represented by the agent set $N = \{1, \dots, n\}$. The i -th agent serves as the ego vehicle and the remaining $n - 1$ agents act as collaborators. All the agents first broadcast basic positional information to their collaborators, including coordinates and heading angle. In this way, the agents obtain the necessary information to project the information from the collaborators’ systems to the ego vehicle’s coordinate system. The ego agent processes its point cloud through a shared encoder to extract Bird’s Eye View (BEV) features, represented as

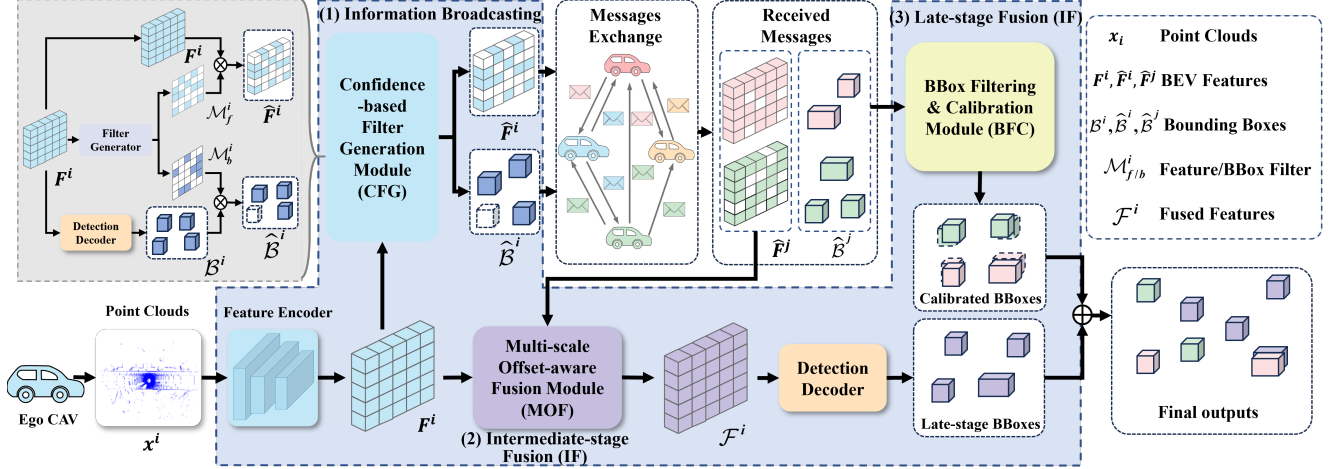


Figure 2. Overview of mmCooper framework: a cooperative perception system with adaptive multi-stage fusion. It consists of three main components: (1) Information Broadcasting (Sec. 3.3) filters features and bounding boxes to achieve bandwidth efficiency; (2) Intermediate-stage Fusion (Sec. 3.4) captures surrounding information from the received feature maps for robust feature fusion; (3) Late-stage Fusion (Sec. 3.5) utilizes the information-rich fused features for Filtering & Calibration of the received bounding boxes.

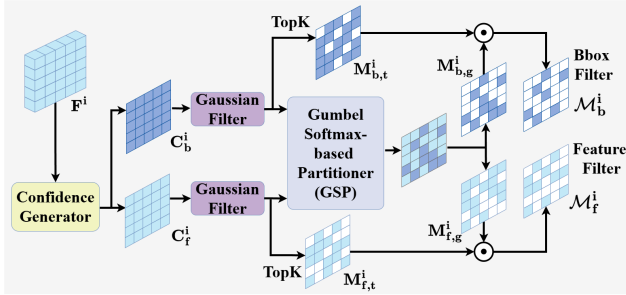


Figure 3. The design of Filter Generator in CFG Module, generating confidence scores to guide information transmission at each location.

$F^i = \psi_E(x^i) \in \mathbb{R}^{C \times H \times W}$, where ψ_E denotes the shared PointPillar [18] encoder, x^i represents the projected local observation, and C , H , and W correspond to the channel, height, and width of the feature map, respectively.

3.3. Information Broadcasting

As shown in the top-left corner of Fig. 2, when conducting information broadcasting, the Confidence-based Filter Generation (CFG) Module dynamically decides whether data at each location should be suppressed, transmitted as intermediate-stage features, or transmitted as late-stage bounding boxes. Notably, no additional model or data compression techniques [32] are applied in this framework, only raw features or bounding boxes are transmitted. The bounding boxes are generated by the Detection Decoder from the features and the transmitting decision is guided by the confidence filter generated by the Filter Generator (Fig. 3) based on the sensing confidence, as detailed below.

Filter Generator. The encoded BEV features (i.e., F^i) are fed into this Confidence Generator to produce intermediate-stage confidence map C_f^i and late-stage confidence map C_b^i .

for all the locations of the scene using CNN. A Gaussian Filter is then applied to the generated confidence maps to smooth out noise and reduce anomalies, improving the selection of critical regions. To suppress the information of the locations with low confidence, only the top $p\%$ highest-confidence positions are selected from each confidence map to generate the spatial filters $M_{f/b,t}^i$ (i.e., $M_{f,t}^i$ or $M_{b,t}^i$). Then, for each location, a classification is required to decide which stage to transmit the data. However, using the traditional Softmax will prevent the back-propagation of the gradient due to its non-differentiability as a discrete operation. Instead, we utilize the Gumbel Softmax [16] to obtain approximate samples from a discrete distribution ensuring the propagation of gradient through the straight-through estimator [2] while preserving standard forward propagation. The Gumbel filter $M_{f/b,g}^i$ obtained in this process is given by the following equation:

$$M_{f/b,g}^i = f_{\max} \left(\frac{\exp((\log C_{f/b} + g_{f/b})/\tau)}{\sum_s \exp((\log C_s + g_s)/\tau)} \right),$$

where $g_{f/b}$ is Gumbel noise [33], τ denotes the temperature parameter of the distribution ($\tau > 0$), and $s \in \{f, b\}$. Based on the above process, our final filter $M_{f/b}^i$ is represented as:

$$M_{f/b}^i = M_{f/b,g}^i \odot M_{f/b,t}^i.$$

Based on the aforementioned filter, the intermediate-stage feature F^i and the coarse bounding box B^i are filtered to obtain the filtered feature \hat{F}^i and coarse bounding box \hat{B}^i .

3.4. Intermediate-stage Fusion

The data shared between agents inevitably contains calibration errors, causing potential misalignment in feature maps. To address this, we propose a Multi-scale Offset-aware Fusion (MOF) Module in the intermediate-stage fusion, which

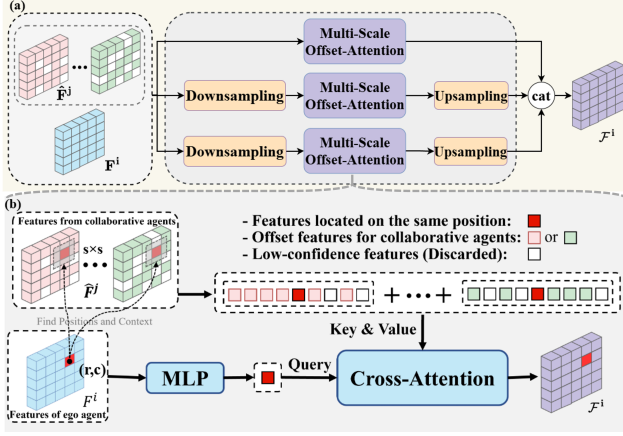


Figure 4. (a) The Multi-scale Offset-aware Fusion Module. (b) The Multi-scale Offset-aware Attention Module.

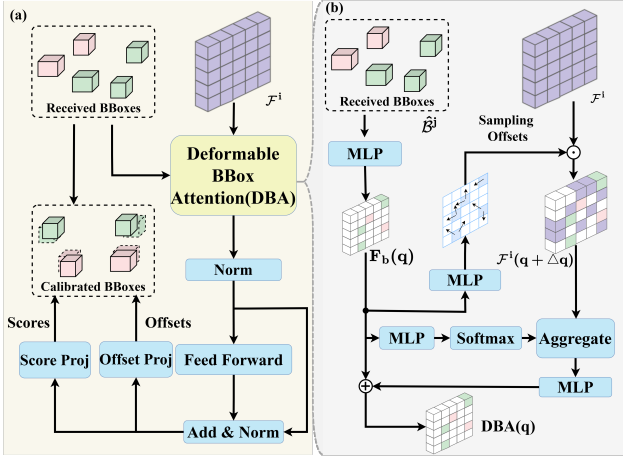


Figure 5. (a) The BBox Filtering & Calibration (BFC) Module. (b) The Deformable BBox Attention (DBA) Module.

aggregates information from neighboring regions, allowing the fusion process at each location to account for potential misalignment. By incorporating the surrounding context, it effectively mitigates the impact of calibration errors, ensuring more accurate and robust agent collaboration.

Multi-scale Offset-aware Fusion (MOF). The overall pipeline of this module is shown in Fig. 4(a). First, the ego features and received collaborator features are encoded at three different scales to capture target information of varying sizes. Next, Multi-scale Offset-aware Attention (MOA) is applied for feature fusion. The features are then upsampled to a uniform size and concatenated across scales to generate the final fused feature F^i .

Multi-scale Offset-aware Attention (MOA). As shown in Fig. 4(b), we encode the ego feature at each location into queries using MLP. Meanwhile, features from a small neighborhood around the corresponding positions in each collaborator’s feature map are extracted as keys and values for cross-attention. Note that low-confidence features are suppressed by collaborators and not transmitted, making

them irrelevant during cross-attention. Specifically, we denote the focused location as (r, c) on the feature map, with a neighborhood size of $s \times s$. The output representation of feature fusion at location (r, c) is expressed as:

$$\mathcal{F}_{r,c}^i = \text{CrossAttn}(\text{MLP}(F_{r,c}^i), \hat{F}_{r,c,s \times s}^j, \hat{F}_{r,c,s \times s}^j),$$

Where $\hat{F}_{r,c,s \times s}^j$ represents the transmitted collaborator features within an $s \times s$ neighborhood centered at position (r, c) . By selectively aggregating the features at this position and its neighborhood, we achieve collaboratively robust feature fusion.

3.5. Late-stage Fusion

The bounding boxes received from collaborators are often redundant, imprecise, misaligned, or even incorrect. To address this, the BBox Filtering & Calibration (BFC) Module in the Late-stage Fusion leverages the information-abundant fused intermediate features to refine the received bounding boxes, either filtering out erroneous ones or correcting their positions for improved accuracy.

BBox Filtering & Calibration (BFC). As depicted in Fig. 5(a), first, the received bounding boxes and the fused intermediate features will be put into the Deformable BBox Attention (DBA) Module as inputs. It then extracts relevant information for each received bounding box from collaborators, which is processed by a vanilla transformer [45] to generate quality scores and positional offsets. Note that, to prevent unreasonable offsets and scores, we bound the output range using the Tanh activation function. Finally, bounding boxes with low quality scores are discarded, while the remaining ones are refined by applying the predicted positional offsets. The refined bounding boxes are then merged with those detected by the ego agent, followed by Non-Maximum Suppression (NMS) to generate the final results. To train the BFC module, we compute the offset loss \mathcal{L}_{off} using the smooth absolute error loss [11] and the score loss \mathcal{L}_{score} using focal loss [24].

Deformable BBox Attention (DBA). As shown in Fig. 5(b), we first encode the received bounding boxes \hat{B}^j by applying an MLP to their coordinates, size, and orientation information to generate feature representations. These features are then mapped onto the BEV space based on the bounding box locations, forming the bounding box feature map $F_b(q)$. To enhance these representations, we employ the deformable cross-attention mechanism to selectively attend to and integrate relevant information from the fused intermediate features. Specifically, the initial bounding box features $F_b(q)$ serve as the query embedding to calculate the offsets of reference points using MLP. Using these offsets, we retrieve the corresponding reference features from the fused intermediate feature map as $F_r^i = \mathcal{F}^i(q + \Delta q_m)$. In the meanwhile, an MLP and Softmax are applied on $F_b(q)$ to generate the aggregation weights for F_r^i , which are then used to weight and integrate the reference features. Finally,

after another MLP layer, we obtain the enhanced bounding box feature map:

$$DBA(q) = \sum_{\alpha=1}^A W_{\alpha} \left[\sum_{n=1}^N \sum_{m=1}^M \omega(W_{\beta} F_b(q)) F_r^i \right] + F_b(q),$$

where A is the number of attention heads, W_{α} and W_{β} are learnable parameters, m represents the number of reference locations, and ω denotes the softmax operation.

3.6. Loss Functions

We use the regression head and classification head of the Detection Decoder [4] to generate the bounding box detection results. The regression results represent the position, size, and yaw angle of each predefined box, expressed as $O_{reg} = f_{dec}^r(\mathcal{F}^i) \in \mathbb{R}^{7 \times H \times W}$. The classification results indicate the confidence score for each predefined box, represented as $O_{cls} = f_{dec}^c(\mathcal{F}^i) \in \mathbb{R}^{2 \times H \times W}$. To optimize the proposed system, we use smooth absolute error loss to supervise regression and focal loss for classification, denoted as \mathcal{L}_{reg} and \mathcal{L}_{cls} , respectively. Combining the previous losses, our total loss is represented as:

$$\mathcal{L}_{total} = \mathcal{L}_{reg} + \mathcal{L}_{cls} + \mathcal{L}_{off} + \mathcal{L}_{score}.$$

4. Experiments

4.1. Datasets and experimental settings

Datasets. We conduct an extensive evaluation on three benchmark datasets, namely OPV2V [50], DAIR-V2X [56], and V2XSet [49]. OPV2V is a large-scale public V2V cooperative perception simulation dataset, which comprises 73 different scenes, 11,464 frames of point clouds and RGB images, and over 230,000 annotated 3D detection boxes. The training, validation, and test sets are divided into 6,374, 1,980, and 2,170 frames, respectively. DAIR-V2X is a large-scale real-world 3D object detection dataset, including 71,254 frames of point cloud and image data, with the training, validation, and test sets split in a 5:2:3 ratio. The V2XSet dataset is a large-scale synthetic dataset designed for V2X perception. It contains a total of 11,447 frames, which is divided into training, validation, and test sets, consisting of 6,694, 1,920, and 2,833 frames, respectively.

Evaluation metrics. To evaluate the 3D object detection performance of the baseline and the proposed framework, we use the average precision (AP) [10] at Intersection-over-Union (IoU) thresholds of 0.5 and 0.7 as the evaluation metric. The communication volume between agents is expressed by the following equation [13]:

$$\mathbf{V} = \log_2 ((|M| \times H \times W \times C + N_b \times 7) \times 32/8),$$

where $|M|$ represents the feature retention ratio, N_b denotes the number of bounding boxes per agent, and 7 is used to describe the coordinates, dimensions, and angle information of each bounding box. Each value is represented using float32, with a division by 8 for bytes.

Table 1. Collaborative perception performance on the OPV2V, DAIR-V2X and V2XSet dataset with a time delay of 100 *ms*, localization errors of 0.2 *m*, and heading errors of 0.2° using Average Precision(AP)@0.7/0.5 as metrics. **Bold numbers** indicate the best results, while underlined numbers represent the second-best results. * represents a variation of PointPillar [18].

Models	OPV2V	DAIR-V2X	V2XSet
	AP@0.7/0.5	AP@0.7/0.5	AP@0.7/0.5
No Fusion* [18]	48.66/68.71	43.57/50.03	40.20/60.60
Late Fusion* [18]	59.48/79.62	34.47/51.14	30.75/54.92
Intermediate Fusion* [18]	<u>70.82/88.41</u>	39.38/56.22	59.38/83.18
When2com [29]	57.55/74.11	33.68/48.20	41.85/67.41
DiscoNet [22]	68.64/84.72	40.69/52.67	54.11/79.82
Where2comm [13]	69.73/85.16	43.71/59.52	<u>63.77/83.17</u>
V2X-ViT [49]	70.06/84.65	40.43/53.08	61.49/83.63
Select2col [28]	62.46/82.30	34.82/51.96	51.22/76.88
ERMVP [58]	69.71/86.63	<u>46.96/64.21</u>	58.44/81.54
Ours	78.11/88.93	48.27/65.12	65.86/84.40

Implementation details. We implement our model on the PyTorch toolbox [35] and train it on NVIDIA GeForce RTX 4090 GPUs. We use the Adam optimizer and adopt batch sizes of 3, 5, and 3 for the OPV2V, DAIR-V2X, and V2XSet datasets, respectively, with 60 epochs for each. All models use the PointPillars [18] backbone to extract features from raw point clouds. The confidence ratio p selected for the CFG module is 70% for OPV2V, 60% for DAIR-V2X, and 70% for V2XSet, and the surrounding grid size chosen for the MOF is 3×3. To closely simulate real traffic conditions, we introduce localization and heading errors with standard deviations of 0.2 *m* and 0.2°, respectively, sampled from a Gaussian distribution. The communication range is limited to 70*m*, excluding agents beyond this range from collaborative communication.

4.2. Quantitative Evaluation

Detection Performance. Tab. 1 presents the comparison of the perception performance of our proposed mmCooper model and various baseline models on OPV2V, DAIR-V2X, and V2XSet datasets with a time delay of 100 *ms*, localization errors of 0.2 *m*, and heading errors of 0.2°. The No Fusion relies solely on ego agent observations. Late Fusion shares only the bounding box results among agents. Intermediate Fusion allows agents to share complete features extracted from raw point clouds. The above three models are all variants based on the PointPillar [18] point cloud detector. Additionally, we consider SOTA models, including When2com [29], DiscoNet [22], Where2comm [13], V2X-ViT [49], Select2col [28] and ERMVP [58]. As shown in the table, our proposed mmCooper outperforms all the baselines on both simulated and real-world datasets. Compared to existing SOTA models, mmCooper outperforms the second-best baseline on the OPV2V, DAIR-V2X, and V2XSet datasets by 7.29%/0.59%, 1.31%/0.91% and 2.09%/0.77% in AP@0.7/0.5, respectively. This demonstrates the effectiveness and superiority of our multi-stage fusion framework.

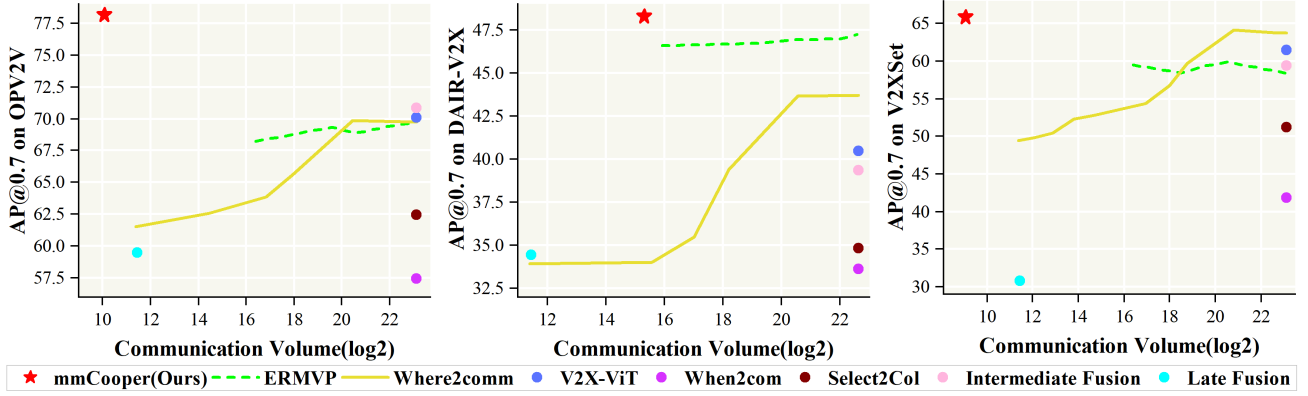


Figure 6. Collaborative perception performance and communication volumes of all the models on the OPV2V, DAIR-V2X, and V2XSet datasets.

Communication Volume. Fig. 6 illustrates the model performance under different bandwidth conditions on the OPV2V, DAIR-V2X, and V2XSet datasets. Experimental results show that mmCooper significantly reduces communication costs, achieving performance levels comparable to late fusion. In comparison to other SOTA models, the communication volume required to achieve optimal performance is 9153/156/18305 times more than our method. Notably, on the OPV2V and V2XSet datasets, our method even achieves lower communication volume than late fusion. This is because our CFG module suppresses low-confidence information from the transmission and selectively transmits complementary and exclusive information at intermediate and late stages rather than transmitting through only one stage encompassing all information of the entire scenario. In addition, since some Late Fusion methods (e.g., OpenCOOD [50]) transmit non-processed (e.g., NMS) BBoxes, our mmCooper even achieves a lower communication volume compared to the late fusion model on certain datasets.

Robustness to Localization Errors and Transmission Delay. We verified the robustness of the agents during collaborative processes in the presence of localization errors and transmission delay on the OPV2V and DAIR-V2X datasets. Following the noise settings in [49], localization noise was sampled from a Gaussian distribution with a mean of $0\ m$ and a standard deviation $\sigma \in \{0, 0.2, 0.4\}m$. As shown in Tab. 2, as the standard deviation of the localization noise gradually increases, the detection performance of the models decreases. On the DAIR-V2X dataset, when2com even performs worse than the No Fusion method when the localization error exceeds $0.2\ m$. Our method outperforms all the baselines under all localization noise settings, demonstrating its robustness to varying levels of localization error. Transmission delay can lead to misalignment of features and proposals, thereby impacting detection performance. We evaluated the models on the OPV2V and DAIR-V2X datasets with time delays $\tau \in \{0, 200, 400\}ms$ set to $0\ ms$, $200\ ms$, and $400\ ms$. With increasing time

delay, the detection performance of all methods gradually degrades. However, mmCooper achieves the highest Average Precision (AP) over all the models on both datasets. This robustness to localization errors and transmission delay demonstrates the effectiveness of the MOF and BFC modules in addressing the potential misalignment and errors during communication among agents. For more results regarding errors during transmission, please refer to the supplementary.

4.3. Ablation Study

We conducted comprehensive ablation studies on the OPV2V and DAIR-V2X datasets to demonstrate the importance of different components, as shown in Tab. 3.

Importance of Core Components. All the core components contribute to performance improvement. Removing the CFG module results in the transmission of information for both the intermediate and late stages across all locations without suppression or selection. While this variant increases the amount of transmitted information compared to mmCooper, it leads to a performance drop. This highlights the importance of filtering out low-confidence information and selectively transmitting data at different stages to optimize performance. The absence of the MOF module replaces the DBA module with a self-attention mechanism, while removing the BFC module eliminates the filtering and refinement of received bounding boxes. Both modifications result in a performance drop, highlighting the importance of incorporating spatial neighborhood information to mitigate misalignment and applying bounding box filtering and refinement to address redundancy, imprecision, or potential errors in received detections.

Superiority of Multi-stage Fusion. We entirely removed the Late Fusion (LF) or the Intermediate Fusion (IF) to degrade our model to single-stage fusion. The experimental results indicate that removing either module leads to a performance decline, underscoring the effectiveness of the proposed multi-stage cooperation framework.

Table 2. Results for different localization errors (m) and transmission delay (ms) on the OPV2V and DAIR-V2X dataset evaluated using AP@0.7. **Bold numbers** indicate the best results, while underlined numbers represent the second-best results.

Noise Type	Localization Errors(m)						Transmission Delay(ms)					
Datasets	OPV2V			DAIR-V2X			OPV2V			DAIR-V2X		
Noise Level	0.0	0.2	0.4	0.0	0.2	0.4	0	200	400	0	200	400
No Fusion	48.66	48.66	48.66	43.57	43.57	43.57	48.66	48.66	48.66	43.57	43.57	43.57
When2com [29]	70.82	64.35	59.98	39.50	36.62	35.03	70.82	43.96	36.55	39.50	36.83	33.72
DiscoNet [22]	76.05	73.59	65.85	46.94	46.03	44.96	76.05	60.08	50.33	46.94	44.03	41.57
Where2comm [13]	78.47	75.45	69.77	52.34	<u>49.34</u>	<u>46.96</u>	78.47	65.23	53.33	52.34	47.76	45.25
V2X-ViT [49]	77.83	75.21	66.72	46.12	43.81	42.53	77.83	66.08	50.33	46.12	45.49	43.99
ERMVP [58]	<u>80.55</u>	<u>76.19</u>	<u>72.78</u>	<u>53.27</u>	48.66	45.97	<u>80.55</u>	<u>68.89</u>	<u>68.31</u>	<u>53.27</u>	<u>49.68</u>	<u>48.60</u>
Ours	86.41	82.53	76.80	56.06	51.52	47.66	86.41	77.44	75.26	56.06	50.96	50.81

Table 3. Ablation study results of different designs in mmCooper on the OPV2V and DAIR-V2X datasets. CFG: Confidence-based Filter Generation Module; MOF: Multi-scale Offset-aware Fusion; BFC: BBox Filtering & Calibration Module; LF: Late-stage Fusion; IF: Intermediate-stage Fusion.

CFG	MOF	BFC	LF	IF	AP@0.7/0.5(\uparrow)	
					OPV2V	DAIR-V2X
✓	✓	✓	✓	✓	78.11/88.93	48.27/65.12
Importance of Core Components						
✗	✓	✓	–	–	73.46/88.84	47.66/63.63
✓	✗	✓	–	–	72.60/88.51	47.27/63.49
✓	✓	✗	–	–	76.77/88.56	44.31/59.68
Results of Single-stage Fusion						
–	–	–	✗	✓	76.83/88.65	46.65/62.84
–	–	–	✓	✗	66.80/78.62	45.78/56.88

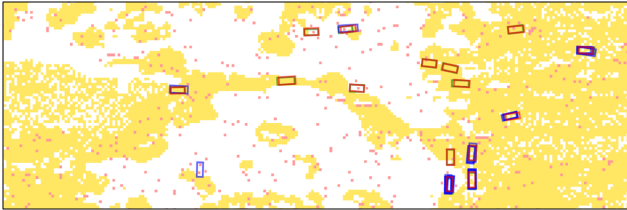


Figure 7. Visualization of two-stage fusion on DAIR-V2X. We show the results from the Confidence-based Filtering Generation Module, including discarded information (white background), BBoxes for transmission (red dots), and features for transmission (yellow background). We also show the BFC module results, including uncalibrated BBoxes (blue boxes), calibrated BBoxes (red boxes), and ground truth BBoxes (green boxes).

4.4. Qualitative Evaluation

Visualization of Two-stage Fusion. As shown in the Fig. 7, we visualize the transmission decisions and bounding boxes refinement in the two-stage fusion on the DAIR-V2X dataset. The yellow background and red dots show the selective transmission of data through two stages. The white background shows the locations discarded by the CFG module, showing a substantial amount of low-confidence or irrelevant information in the scenario. The removal and correction of the uncalibrated blue boxes demonstrates the BFC module’s effectiveness in filtering and refining received bounding boxes by eliminating redundancies and improving alignment with the ground truth.

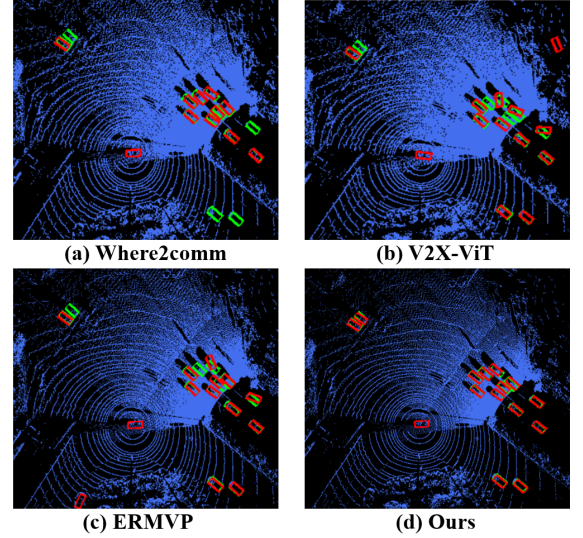


Figure 8. Visualization comparison of detection results on the DAIR-V2X dataset. Green and red boxes represent the ground truth and the model-predicted bounding boxes, respectively.

Visualization of Detection Results. Fig. 8 shows visualization results for a scenario in the DAIR-V2X dataset. Compared to baseline methods, mmCooper demonstrates high-precision 3D object detection, accurately predicting nearly all ground truth objects. In contrast, baseline methods either fail to detect certain vehicles or produce inaccurate bounding boxes. Refer to the supplementary materials for additional visualized detection results.

5. Conclusion

In this paper, we have proposed mmCooper, a novel multi-agent, multi-stage, communication-efficient, and collaboration-robust cooperative perception framework. mmCooper is the first framework to achieve adaptive fusion of complementary data across stages for cooperative perception. We introduce the Confidence-based Filter Generation Module to enable dynamic partitioning of intermediate features and late-stage bounding boxes, balancing communication load and perception performance. Additionally, the Multi-scale Offset-aware Fusion module and BBox Filtering & Calibration module are incorporated to address potential misalignment and calibration noise

among agents. mmCooper outperforms the second-best state-of-the-art models on the OPV2V, DAIR-V2X, and V2Xset datasets, achieving improvements of 7.29%, 1.31%, and 2.09% in AP@0.7, respectively, while reducing communication volume by factors of 9153, 156 and 18305.

References

- [1] Christoph Allig and Gerd Wanielik. Alignment of perception information for cooperative perception. In *2019 IEEE Intelligent Vehicles Symposium (IV)*, pages 1849–1854. IEEE, 2019. 1
- [2] Yoshua Bengio, Nicholas Léonard, and Aaron Courville. Estimating or propagating gradients through stochastic neurons for conditional computation. *arXiv preprint arXiv:1308.3432*, 2013. 4
- [3] Kunyang Cai, Ting Qu, Bingzhao Gao, and Hong Chen. Consensus-based distributed cooperative perception for connected and automated vehicles. *IEEE Transactions on Intelligent Transportation Systems*, 24(8):8188–8208, 2023. 2
- [4] Nicolas Carion, Francisco Massa, Gabriel Synnaeve, Nicolas Usunier, Alexander Kirillov, and Sergey Zagoruyko. End-to-end object detection with transformers. In *European conference on computer vision*, pages 213–229. Springer, 2020. 6
- [5] Cheng Chang, Jiawei Zhang, Kunpeng Zhang, Wenqin Zhong, Xinyu Peng, Shen Li, and Li Li. Bev-v2x: Cooperative birds-eye-view fusion and grid occupancy prediction via v2x-based data sharing. *IEEE Transactions on Intelligent Vehicles*, 2023. 1
- [6] Guoying Chen, Xuanming Zhao, Zhenhai Gao, and Min Hua. Dynamic drifting control for general path tracking of autonomous vehicles. *IEEE Transactions on Intelligent Vehicles*, 8(3):2527–2537, 2023. 1
- [7] Qi Chen, Sihai Tang, Qing Yang, and Song Fu. Cooper: Cooperative perception for connected autonomous vehicles based on 3d point clouds. In *2019 IEEE 39th International Conference on Distributed Computing Systems (ICDCS)*, pages 514–524. IEEE, 2019. 1, 2
- [8] Ziming Chen, Yifeng Shi, and Jinrang Jia. Transiff: An instance-level feature fusion framework for vehicle-infrastructure cooperative 3d detection with transformers. In *Proceedings of the IEEE/CVF International Conference on Computer Vision*, pages 18205–18214, 2023. 1
- [9] Abhishek Das, Théophile Gervet, Joshua Romoff, Dhruv Batra, Devi Parikh, Mike Rabbat, and Joelle Pineau. Tarmac: Targeted multi-agent communication. In *International Conference on machine learning*, pages 1538–1546. PMLR, 2019. 2
- [10] Mark Everingham, Luc Van Gool, Christopher KI Williams, John Winn, and Andrew Zisserman. The pascal visual object classes (voc) challenge. *International journal of computer vision*, 88:303–338, 2010. 6
- [11] Ross Girshick. Fast r-cnn. In *Proceedings of the IEEE international conference on computer vision*, pages 1440–1448, 2015. 5
- [12] Yedid Hoshen. Vain: Attentional multi-agent predictive modeling. *Advances in neural information processing systems*, 30, 2017. 2
- [13] Yue Hu, Shaoheng Fang, Zixing Lei, Yiqi Zhong, and Siheng Chen. Where2comm: Communication-efficient collaborative perception via spatial confidence maps. *Advances in neural information processing systems*, 35:4874–4886, 2022. 1, 3, 6, 8
- [14] Min Hua, Guoying Chen, Buyang Zhang, and Yanjun Huang. A hierarchical energy efficiency optimization control strategy for distributed drive electric vehicles. *Proceedings of the Institution of Mechanical Engineers, Part D: Journal of Automobile Engineering*, 233(3):605–621, 2019. 1
- [15] Tao Huang, Jianan Liu, Xi Zhou, Dinh C Nguyen, Mostafa Rahimi Azghadi, Yuxuan Xia, Qing-Long Han, and Sumei Sun. V2x cooperative perception for autonomous driving: Recent advances and challenges. *arXiv preprint arXiv:2310.03525*, 2023. 1
- [16] Eric Jang, Shixiang Gu, and Ben Poole. Categorical reparameterization with gumbel-softmax. *arXiv preprint arXiv:1611.01144*, 2016. 4
- [17] Jiechuan Jiang and Zongqing Lu. Learning attentional communication for multi-agent cooperation. *Advances in neural information processing systems*, 31, 2018. 2
- [18] Alex H Lang, Sourabh Vora, Holger Caesar, Lubing Zhou, Jiong Yang, and Oscar Beijbom. Pointpillars: Fast encoders for object detection from point clouds. In *Proceedings of the IEEE/CVF conference on computer vision and pattern recognition*, pages 12697–12705, 2019. 4, 6
- [19] Jesse Levinson, Jake Askeland, Jan Becker, Jennifer Dolson, David Held, Soeren Kammel, J Zico Kolter, Dirk Langer, Oliver Pink, Vaughan Pratt, et al. Towards fully autonomous driving: Systems and algorithms. In *2011 IEEE intelligent vehicles symposium (IV)*, pages 163–168. IEEE, 2011. 1
- [20] Jinlong Li, Runsheng Xu, Xinyu Liu, Jin Ma, Zicheng Chi, Jiaqi Ma, and Hongkai Yu. Learning for vehicle-to-vehicle cooperative perception under lossy communication. *IEEE Transactions on Intelligent Vehicles*, 8(4):2650–2660, 2023. 2
- [21] Yiming Li, Bir Bhanu, and Wei Lin. Auction protocol for camera active control. In *2010 IEEE International Conference on Image Processing*, pages 4325–4328. IEEE, 2010. 2
- [22] Yiming Li, Shunli Ren, Pengxiang Wu, Siheng Chen, Chen Feng, and Wenjun Zhang. Learning distilled collaboration graph for multi-agent perception. *Advances in Neural Information Processing Systems*, 34:29541–29552, 2021. 2, 3, 6, 8, 1
- [23] Zhiqi Li, Wenhai Wang, Hongyang Li, Enze Xie, Chonghao Sima, Tong Lu, Yu Qiao, and Jifeng Dai. Bevformer: Learning bird’s-eye-view representation from multi-camera images via spatiotemporal transformers. In *European conference on computer vision*, pages 1–18. Springer, 2022. 1
- [24] Tsung-Yi Lin, Priya Goyal, Ross Girshick, Kaiming He, and Piotr Dollár. Focal loss for dense object detection. In *Proceedings of the IEEE international conference on computer vision*, pages 2980–2988, 2017. 5
- [25] Bingyi Liu, Weizhen Han, Enshu Wang, Shengwu Xiong, Chunming Qiao, and Jianping Wang. An efficient message

- dissemination scheme for cooperative drivings via cooperative hierarchical attention reinforcement learning. *IEEE Transactions on Mobile Computing*, 2023. 1
- [26] Bingyi Liu, Jingxiang Hao, Enshu Wang, Dongyao Jia, Weizhen Han, Libing Wu, and Shengwu Xiong. Multi-agent reinforcement learning based resource allocation for efficient message dissemination in c-v2x networks. In *2024 IEEE/ACM 32nd International Symposium on Quality of Service (IWQoS)*, pages 1–10. IEEE, 2024. 1
- [27] Wei Liu, Lu Xiong, Xin Xia, Yishi Lu, Letian Gao, and Shunhui Song. Vision-aided intelligent vehicle sideslip angle estimation based on a dynamic model. *IET Intelligent Transport Systems*, 14(10):1183–1189, 2020. 1
- [28] Yuntao Liu, Qian Huang, Rongpeng Li, Xianfu Chen, Zhifeng Zhao, Shuyuan Zhao, Yongdong Zhu, and Honggang Zhang. Select2col: Leveraging spatial-temporal importance of semantic information for efficient collaborative perception. *IEEE Transactions on Vehicular Technology*, 2024. 6, 3
- [29] Yen-Cheng Liu, Junjiao Tian, Nathaniel Glaser, and Zsolt Kira. When2com: Multi-agent perception via communication graph grouping. In *Proceedings of the IEEE/CVF Conference on computer vision and pattern recognition*, pages 4106–4115, 2020. 2, 3, 6, 8, 1
- [30] Zhijian Liu, Haotian Tang, Alexander Amini, Xinyu Yang, Huizi Mao, Daniela L Rus, and Song Han. Bevfusion: Multi-task multi-sensor fusion with unified bird’s-eye view representation. In *2023 IEEE international conference on robotics and automation (ICRA)*, pages 2774–2781. IEEE, 2023. 1
- [31] Yifan Lu, Quanhao Li, Baoan Liu, Mehrdad Dianati, Chen Feng, Siheng Chen, and Yanfeng Wang. Robust collaborative 3d object detection in presence of pose errors. In *2023 IEEE International Conference on Robotics and Automation (ICRA)*, pages 4812–4818. IEEE, 2023. 1
- [32] Yunsheng Ma, Juanwu Lu, Can Cui, Sicheng Zhao, Xu Cao, Wenqian Ye, and Ziran Wang. Macp: Efficient model adaptation for cooperative perception. In *Proceedings of the IEEE/CVF Winter Conference on Applications of Computer Vision (WACV)*, pages 3373–3382, 2024. 4
- [33] Chris J Maddison, Andriy Mnih, and Yee Whye Teh. The concrete distribution: A continuous relaxation of discrete random variables. *arXiv preprint arXiv:1611.00712*, 2016. 4
- [34] Zhenyang Ni, Zixing Lei, Yifan Lu, Dingju Wang, Chen Feng, Yanfeng Wang, and Siheng Chen. Self-localized collaborative perception. *arXiv preprint arXiv:2406.12712*, 2024. 1
- [35] Adam Paszke, Sam Gross, Francisco Massa, Adam Lerer, James Bradbury, Gregory Chanan, Trevor Killeen, Zeming Lin, Natalia Gimelshein, Luca Antiga, et al. Pytorch: An imperative style, high-performance deep learning library. *Advances in neural information processing systems*, 32, 2019. 6
- [36] Andrea Piazzoni, Jim Cherian, Roshan Vijay, Lap-Pui Chau, and Justin Dauwels. Copem: Cooperative perception error models for autonomous driving. In *2022 IEEE 25th International Conference on Intelligent Transportation Systems (ITSC)*, pages 3934–3939. IEEE, 2022. 2
- [37] Faisal Qureshi and Demetri Terzopoulos. Smart camera networks in virtual reality. *Proceedings of the IEEE*, 96(10):1640–1656, 2008. 2
- [38] Shuyao Shi, Jiahe Cui, Zhehao Jiang, Zhenyu Yan, Guoliang Xing, Jianwei Niu, and Zhenchao Ouyang. Vips: Real-time perception fusion for infrastructure-assisted autonomous driving. In *Proceedings of the 28th annual international conference on mobile computing and networking*, pages 133–146, 2022. 1, 2
- [39] Amanpreet Singh, Tushar Jain, and Sainbayer Sukhbaatar. Learning when to communicate at scale in multiagent cooperative and competitive tasks. *arXiv preprint arXiv:1812.09755*, 2018. 2
- [40] Zhiying Song, Fuxi Wen, Hailiang Zhang, and Jun Li. A cooperative perception system robust to localization errors. In *2023 IEEE Intelligent Vehicles Symposium (IV)*, pages 1–6. IEEE, 2023. 1, 2
- [41] Hao Su, Shin’ichi Arakawa, and Masayuki Murata. 3d multi-object tracking based on two-stage data association for collaborative perception scenarios. In *2023 IEEE Intelligent Vehicles Symposium (IV)*, pages 1–7. IEEE, 2023. 1
- [42] Sanbao Su, Songyang Han, Yiming Li, Zhili Zhang, Chen Feng, Caiwen Ding, and Fei Miao. Collaborative multi-object tracking with conformal uncertainty propagation. *IEEE Robotics and Automation Letters*, 2024. 2
- [43] Sainbayer Sukhbaatar, Rob Fergus, et al. Learning multi-agent communication with backpropagation. *Advances in neural information processing systems*, 29, 2016. 2
- [44] Ming Tan. Multi-agent reinforcement learning: Independent vs. cooperative agents. In *Proceedings of the tenth international conference on machine learning*, pages 330–337, 1993. 2
- [45] A Vaswani. Attention is all you need. *Advances in Neural Information Processing Systems*, 2017. 5
- [46] Tsun-Hsuan Wang, Sivabalan Manivasagam, Ming Liang, Bin Yang, Wenyan Zeng, and Raquel Urtasun. V2vnet: Vehicle-to-vehicle communication for joint perception and prediction. In *Computer Vision—ECCV 2020: 16th European Conference, Glasgow, UK, August 23–28, 2020, Proceedings, Part II 16*, pages 605–621. Springer, 2020. 1
- [47] Sizhe Wei, Yuxi Wei, Yue Hu, Yifan Lu, Yiqi Zhong, Siheng Chen, and Ya Zhang. Asynchrony-robust collaborative perception via bird’s eye view flow. *Advances in Neural Information Processing Systems*, 36, 2024. 1
- [48] Qi Xie, Xiaobo Zhou, Tie Qiu, Qingyu Zhang, and Wenyu Qu. Soft actor-critic-based multilevel cooperative perception for connected autonomous vehicles. *IEEE Internet of Things Journal*, 9(21):21370–21381, 2022. 3
- [49] Runsheng Xu, Hao Xiang, Zhengzhong Tu, Xin Xia, Ming-Hsuan Yang, and Jiaqi Ma. V2x-vit: Vehicle-to-everything cooperative perception with vision transformer. In *European conference on computer vision*, pages 107–124. Springer, 2022. 2, 3, 6, 7, 8, 1
- [50] Runsheng Xu, Hao Xiang, Xin Xia, Xu Han, Jinlong Li, and Jiaqi Ma. Opv2v: An open benchmark dataset and fusion pipeline for perception with vehicle-to-vehicle communication. In *2022 International Conference on Robotics and Automation (ICRA)*, pages 2583–2589. IEEE, 2022. 2, 6, 7, 1

- [51] Runsheng Xu, Weizhe Chen, Hao Xiang, Xin Xia, Lantao Liu, and Jiaqi Ma. Model-agnostic multi-agent perception framework. In *2023 IEEE International Conference on Robotics and Automation (ICRA)*, pages 1471–1478. IEEE, 2023. [2](#)
- [52] Chenyu Yang, Yuntao Chen, Hao Tian, Chenxin Tao, Xizhou Zhu, Zhaoxiang Zhang, Gao Huang, Hongyang Li, Yu Qiao, Lewei Lu, et al. Bevformer v2: Adapting modern image backbones to bird’s-eye-view recognition via perspective supervision. In *Proceedings of the IEEE/CVF Conference on Computer Vision and Pattern Recognition*, pages 17830–17839, 2023. [1](#)
- [53] Dingkan Yang, Kun Yang, Yuzheng Wang, Jing Liu, Zhi Xu, Rongbin Yin, Peng Zhai, and Lihua Zhang. How2comm: Communication-efficient and collaboration-pragmatic multi-agent perception. *Advances in Neural Information Processing Systems*, 36, 2024. [1](#)
- [54] Kun Yang, Dingkan Yang, Jingyu Zhang, Mingcheng Li, Yang Liu, Jing Liu, Hanqi Wang, Peng Sun, and Liang Song. Spatio-temporal domain awareness for multi-agent collaborative perception. In *Proceedings of the IEEE/CVF International Conference on Computer Vision*, pages 23383–23392, 2023.
- [55] Kun Yang, Dingkan Yang, Jingyu Zhang, Hanqi Wang, Peng Sun, and Liang Song. What2comm: Towards communication-efficient collaborative perception via feature decoupling. In *Proceedings of the 31st ACM International Conference on Multimedia*, pages 7686–7695, 2023. [1](#)
- [56] Haibao Yu, Yizhen Luo, Mao Shu, Yiyi Huo, Zebang Yang, Yifeng Shi, Zhenglong Guo, Hanyu Li, Xing Hu, Jirui Yuan, et al. Dair-v2x: A large-scale dataset for vehicle-infrastructure cooperative 3d object detection. In *Proceedings of the IEEE/CVF Conference on Computer Vision and Pattern Recognition*, pages 21361–21370, 2022. [2](#), [6](#), [1](#)
- [57] Ekim Yurtsever, Jacob Lambert, Alexander Carballo, and Kazuya Takeda. A survey of autonomous driving: Common practices and emerging technologies. *IEEE access*, 8:58443–58469, 2020. [1](#)
- [58] Jingyu Zhang, Kun Yang, Yilei Wang, Hanqi Wang, Peng Sun, and Liang Song. Ermvp: Communication-efficient and collaboration-robust multi-vehicle perception in challenging environments. In *Proceedings of the IEEE/CVF Conference on Computer Vision and Pattern Recognition*, pages 12575–12584, 2024. [3](#), [6](#), [8](#), [1](#)
- [59] Qingzhao Zhang, Xumiao Zhang, Ruiyang Zhu, Fan Bai, Mohammad Naserian, and Z Morley Mao. Robust real-time multi-vehicle collaboration on asynchronous sensors. In *Proceedings of the 29th Annual International Conference on Mobile Computing and Networking*, pages 1–15, 2023. [2](#)
- [60] Qingzhao Zhang, Shuowei Jin, Ruiyang Zhu, Jiachen Sun, Xumiao Zhang, Qi Alfred Chen, and Z Morley Mao. On data fabrication in collaborative vehicular perception: Attacks and countermeasures. In *33rd USENIX Security Symposium (USENIX Security 24)*, pages 6309–6326, 2024. [3](#)
- [61] Xumiao Zhang, Anlan Zhang, Jiachen Sun, Xiao Zhu, Y Ethan Guo, Feng Qian, and Z Morley Mao. Emp: Edge-assisted multi-vehicle perception. In *Proceedings of the 27th*

mmCooper: A Multi-agent Multi-stage Communication-efficient and Collaboration-robust Cooperative Perception Framework

Supplementary Material

1. Overview

The supplementary material is organized into the following sections:

- Sec. 2: The System Pipeline of mmCooper
- Sec. 3: Additional Experimental Results on OPV2V and DAIR-V2X Datasets
 - Sec. 3.1: Implementation Details
 - Sec. 3.2: Supplements on Localization Errors
 - Sec. 3.3: Supplements on Transmission Delays
 - Sec. 3.4: Robustness to Heading Errors
 - Sec. 3.5: Computation Costs
- Sec. 4: Additional Qualitative Evaluation Results
 - Sec. 4.1: Visualization of Detection Result
 - Sec. 4.2: Visualization of Multi-stage Fusion

2. The System Pipeline of mmCooper

The proposed system pipeline of mmCooper is illustrated in Algorithm 1. Note that the following pipeline is executed in parallel across all agents. For simplicity, we describe the pipeline from the perspective of the ego agent. The ego agent is represented by i , while the collaborative agents are denoted by j . First, the agent generates BEV features F^i and F^j through the Observation Encoding. In the Information Broadcasting, agents generate initial coarse bounding boxes B^i and B^j , where N_{bbx}^i and N_{bbx}^j represent the number of bounding boxes predicted by the ego agent and the collaborating agents, respectively. The collaborative agents then package and broadcast the filtered BEV features along with the coarse bounding boxes. Specifically, $f_{gaussian}(\cdot)$ denotes a Gaussian filter, and $\{\hat{F}^j, \hat{B}^j\}$ represents the filtered features and bounding boxes from the collaborative agents.

Subsequently, in the Intermediate-stage Fusion, the ego agent performs feature fusion using the Multi-scale Offset-aware Attention module. The outputs from the fused features at different scales, after undergoing upsampling, are concatenated to obtain the final fused features. Here, $f_{up2}(\cdot)$ and $f_{up3}(\cdot)$ denote the upsampling operations, while $\{F_{sc1}^i, F_{sc2}^i, F_{sc3}^i\}$ represent the feature fusion outputs at three different scales.

In the later-stage fusion, the BBox Filtering & Calibration Module is employed to learn the bounding box offsets and scores. Specifically, DBA refers to the Deformable Bounding Boxes Attention Module, while FFN denotes the feed-forward network, $f_{enc,b}(\cdot)$ represents the feature extractor for bounding boxes, $f_{off}(\cdot)$ is the offset mapping

function, and $f_{score}(\cdot)$ is the score mapping function. $\varphi(\cdot)$ represents the filtering and calibration through scores and offsets.

Finally, the fused features are input into a detection head to predict the fused bounding box B_{fused} . The final bounding box is composed of the bounding box predicted from the fused features B_{fused} and the bounding box obtained after filtering and calibration \hat{B}_m^j from collaborative agents. $f_{post}(\cdot)$ represents the combination of all bounding boxes.

3. Additional Experimental Results on OPV2V and DAIR-V2X Datasets

In this section, we provide additional experiments to supplement the results on the datasets OPV2V[50] and DAIR-V2X[56] presented in the *main paper*.

3.1. Implementation Details

On the OPV2V and DAIR-V2X datasets, the dimensions of the voxels encoded by the encoder are $0.4 \times 0.4 \times 4$. The shape of the shared BEV features among agents is (64, 100, 252) for DAIR-V2X and (64, 100, 352) for OPV2V. The shared bounding boxes among agents are represented by their center coordinates, dimensions (length, width, height), and heading angle. The detection decoder consists of two distinct 1×1 convolutional layers.

3.2. Supplements on Localization Errors

The localization errors on the OPV2V and DAIR-V2X datasets are sampled from a Gaussian distribution with a mean of 0 m and a standard deviation $\sigma \in \{0.0, 0.1, 0.2, 0.3, 0.4\}m$. The experimental results, as shown in Fig. 9, demonstrate that our proposed mmCooper outperforms the existing state-of-the-art methods[13, 22, 29, 49, 58] across different levels of localization error, highlighting its robustness to such errors.

3.3. Supplements on Transmission Delays

We evaluated the performance of the models on the OPV2V and DAIR-V2X datasets under transmission delays for $\{0, 100, 200, 300, 400\}ms$. As shown in Fig. 10, our proposed mmCooper consistently outperforms the existing state-of-the-art methods across all transmission delay conditions, demonstrating the superiority of our approach in scenarios with transmission delays.

Algorithm 1 System Pipeline of the Proposed mmCooper

Define $N = \{1, \dots, n\}$ as the agent set, $i \in N$ represents the ego agent, while $j \in N$ denotes the collaborative agents. $x_{i/j}$ serves as the input point cloud.

—
For collaborative agents.

Observation Encoding.

for each agent $j \in N$, **do**

$$F^j = \psi_{encoder}(x^j) \in \mathbb{R}^{C \times H \times W}$$

end for

Information Broadcasting.

for each $j \in N$, **do**

$$\mathcal{B}^j = f_{dec}(F^j) \in \mathbb{R}^{N_{bbx}^j \times 7}$$

$$C_f^j, C_b^j = \phi_{conf}(F^j)$$

$$C_f^j, C_b^j = f_{gaussian}(C_f^j, C_b^j)$$

$$M_{f,top}^j, M_{b,top}^j = f_{top}(C_f^j, C_b^j)$$

$$M_{f,g}^j, M_{b,g}^j = f_{max}\left(\frac{\exp((\log C_{f/b}^j + g_f)/\tau)}{\sum_s \exp((\log C_s^j + g_s)/\tau)}\right)$$

$$\mathcal{M}_{f/b}^j = M_{f/b,g}^j \odot M_{f/b,top}^j$$

$$\hat{F}^j = \mathcal{M}_f^j \odot F^j; \hat{B}^j = \mathcal{M}_b^j \odot B^j$$

broadcast $\{\hat{F}^j, \hat{B}^j\}$ to other agent

end for

—
For ego agent.

Observation Encoding.

$$F^i = \psi_{encoder}(x^i) \in \mathbb{R}^{C \times H \times W}$$

Information Broadcasting.

$$\mathcal{B}^i = f_{dec}(F^i) \in \mathbb{R}^{N_{bbx}^i \times 7}$$

Intermediate-stage Fusion.

Receive $\{\hat{F}^j, \hat{B}^j\}$ sent by collaborative agents.

Encode the feature set $\{F^i, \hat{F}^j\}$ into three scales $S = \{sc1, sc2, sc3\}$.

For each $sc \in S$, **do**

$$\mathcal{F}_{sc,(r,c)}^i = CrossAttn(\sigma(F_{sc,(r,c)}^i), \hat{F}_{sc,(r,c)}^{j,s \times s}, \hat{B}_{sc,(r,c)}^{j,s \times s})$$

end for

$$\mathcal{F}^i = concat(\mathcal{F}_{sc1}^i, f_{up2}(\mathcal{F}_{sc2}^i), f_{up3}(\mathcal{F}_{sc3}^i))$$

Late-stage Fusion.

$$F_b(q) = f_{enc,b}(\hat{B}^j)$$

$$DBA(q) = \sum_{\alpha=1}^A W_{\alpha} [\sum_{n=1}^N \sum_{m=1}^M \omega(W_{\beta} F_b(q)) \mathcal{F}^i(q + \Delta q_m)]$$

$$F_{DBA} = DBA(q) + \mathcal{F}^i$$

$$F_{DBA} = FFN(F_{DBA}) + F_{DBA}$$

$$off, score = f_{off}(F_{DBA}), f_{score}(F_{DBA})$$

$$\hat{B}_m^j = \varphi(off, score, \hat{B}^j)$$

Detection Decoders

$$\mathcal{B}_{fused} = f_{dec}(\mathcal{F}^i)$$

$$\mathcal{B}_{final}^i = f_{post}(B^i, \hat{B}_m^j, \mathcal{B}_{fused})$$

3.4. Robustness to Heading Errors.

Fig. 11 demonstrates the performance of our proposed mmCooper method compared to other baseline methods under varying levels (i.e., $\{0.0, 0.2, 0.4, 0.6, 0.8\}^\circ$) of heading er-

ror noise on the OPV2V and DAIR-V2X datasets. As illustrated in Fig. 11, the performance of all models decreases as the heading errors increase. However, mmCooper consistently outperforms the current state-of-the-art models across

Models	OPV2V
	Inference Time(ms)
Intermediate Fusion*	10.07
Where2comm [13]	17.05
V2X-ViT [49]	114.11
Select2col [28]	27.00
ERMVP [58]	55.30
Ours	45.41

Module	OPV2V
	Inference Time(ms)
Observation Encoding	12.26
Information Broadcasting	14.37
Intermediate-stage Fusion	13.54
Late-stage Fusion	4.06
mmCooper	45.41

Table 4. The left table presents the inference time of different models on the OPV2V dataset, while the right table shows the inference time of different components in mmCooper.

all error levels, highlighting the advantages of our designed Multi-Scale Offset-Aware Fusion Module and BBox Filtering & Calibration Module in enhancing system robustness.

3.5. Computation Costs

Tab. 4 presents the overall computation time of our model as well as the computation time of each module. Although both our intermediate-stage and late-stage fusion modules utilize attention-based mechanisms, due to the sparsity of intermediate-stage features from collaborators and the sparsity of reference points used in deformable attention during late-stage fusion, our model achieves inference time comparable to other models.

4. Additional Qualitative Evaluation Results

4.1. Visualization of Detection Result

We provide additional qualitative results on DAIR-V2X datasets. Fig. 13 present visualizations of different road scenarios. Our proposed mmCooper method can detect almost all ground truths without any false positives. The results demonstrate that our proposed mmCooper achieves outstanding detection performance across various scenarios.

4.2. Visualization of Multi-stage Fusion

We provide more visualizations for multi-stage fusion in different scenarios. As shown in the Fig. 12, our mmCooper effectively performs dynamic allocation of intermediate-stage features and late-stage bounding boxes across different scenarios while also refining the received bounding boxes.

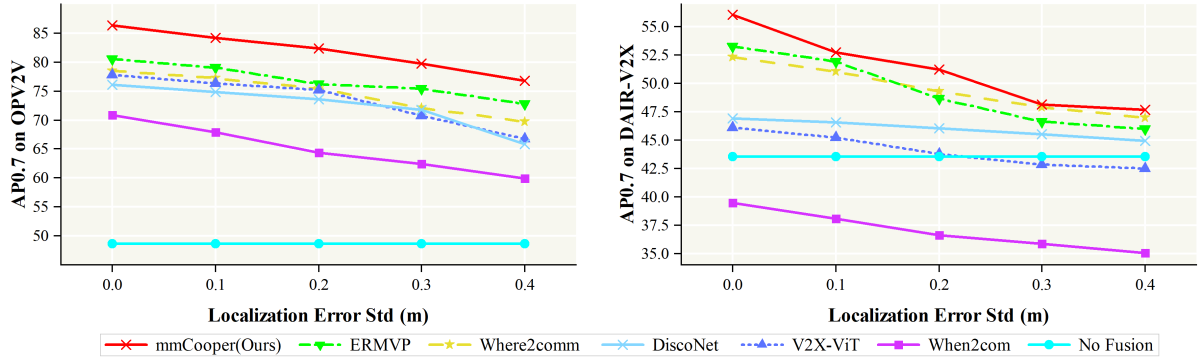


Figure 9. Robustness to the localization error on the OPV2V and DAIR-V2X datasets.

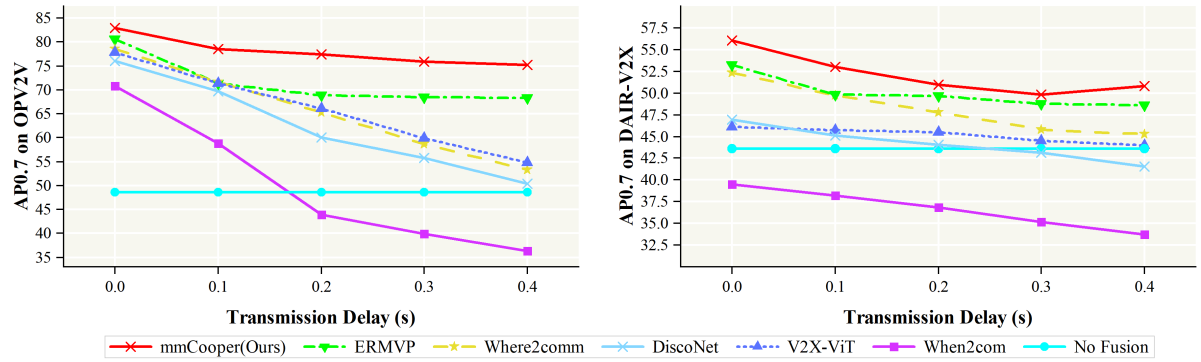


Figure 10. Robustness to the transmission delay on the OPV2V and DAIR-V2X datasets.

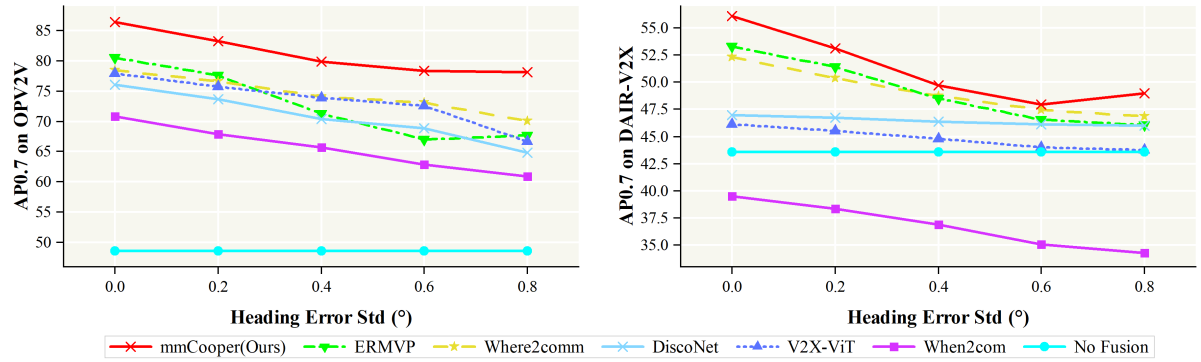


Figure 11. Robustness to the heading error on the OPV2V and DAIR-V2X datasets.

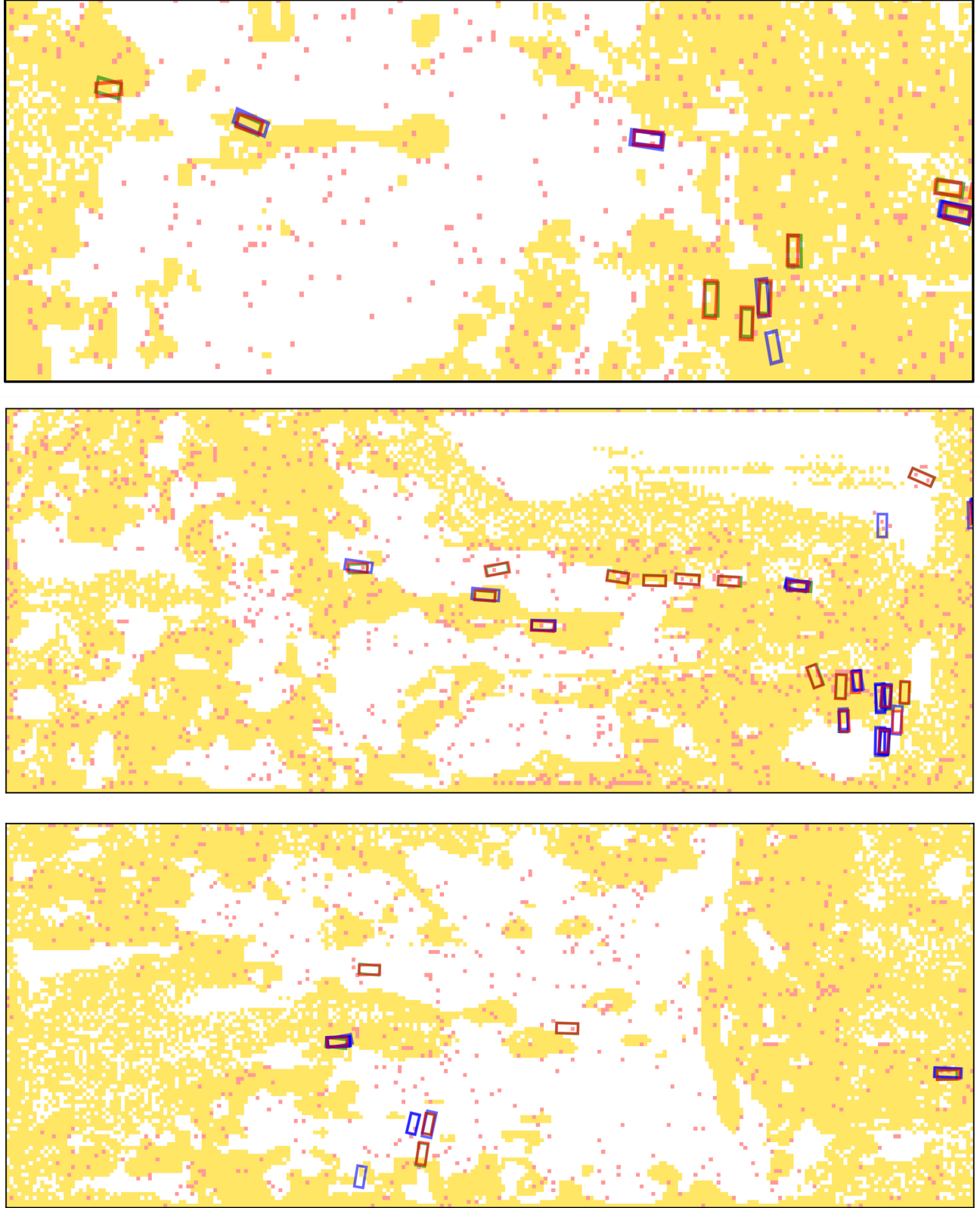


Figure 12. Visualization of two-stage fusion on DAIR-V2X. We show the results from the Confidence-based Filtering Generation Module, including discarded information (white background), BBoxes for transmission (red dots), and features for transmission (yellow background). We also show the BFC module results, including uncalibrated BBoxes (blue boxes), calibrated BBoxes (red boxes), and ground truth BBoxes (green boxes).

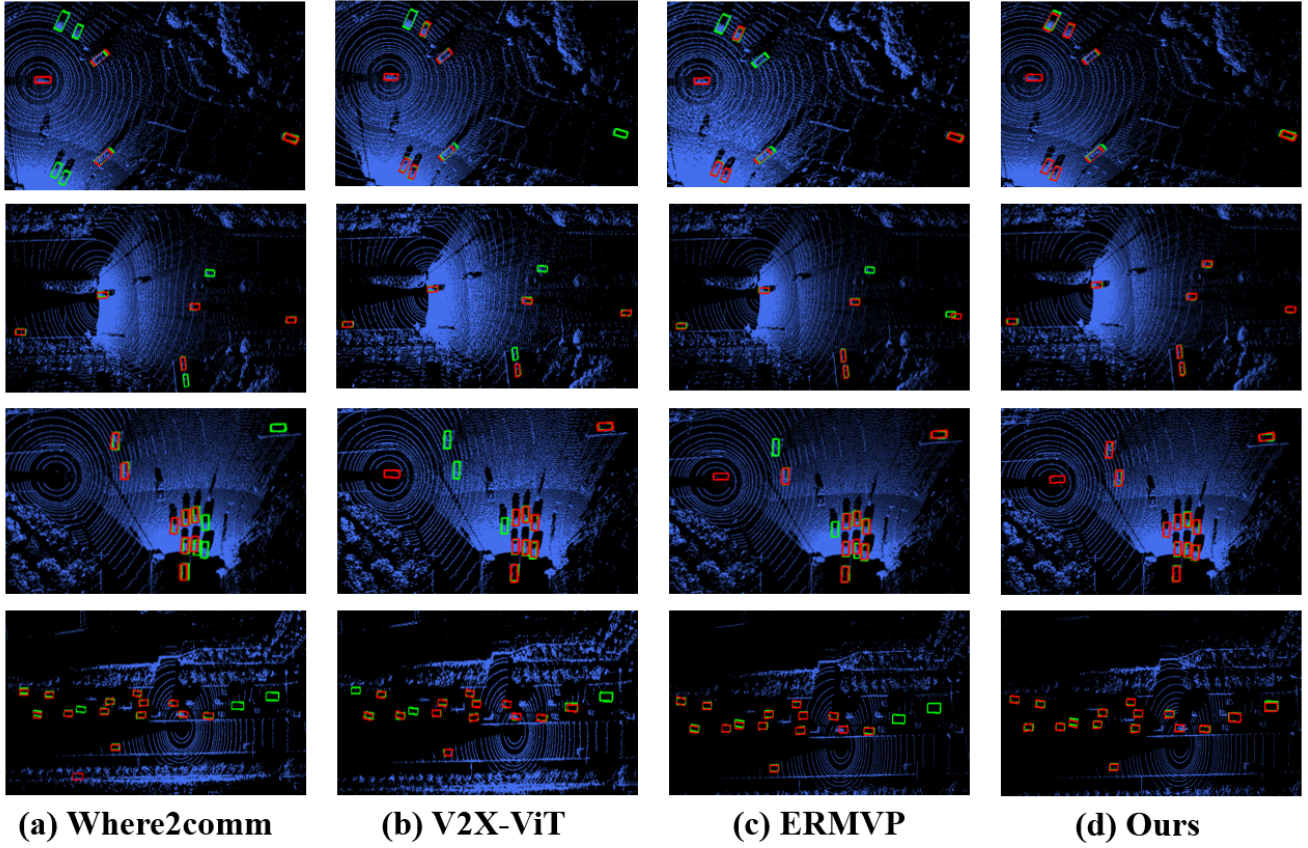


Figure 13. More visualization comparison of detection results on the DAIR-V2X dataset. Green and red boxes represent the ground truth and the model-predicted bounding boxes, respectively.